ASME Open Journal of Engineering
Online journal at:
https://asmedigitalcollection.asme.org/openengineering

Optimizing Supercritical Carbon Dioxide Cycles Performance With Respect to Split Ratio and Intermediate Pressure

Akif Eren Tatli[1]
Department of Mechanical and Industrial Engineering,
Northeastern University,
Boston, MA 02115
e-mail: tatli.a@northeastern.edu

Dongchuan You
Department of Mechanical and Industrial Engineering,
Northeastern University,
Boston, MA 02115
e-mail: you.d@northeastern.edu

Hameed Metghalchi
Life Fellow ASME
Department of Mechanical and Industrial Engineering,
Northeastern University,
Boston, MA 02115
e-mail: metghalchi@coe.neu.edu

Supercritical carbon dioxide power cycles are getting more attention every day due to their high efficiencies. This study has examined determination of split ratio and intermediate pressure for maximum efficiency in various supercritical carbon dioxide recompression cycle configurations. Five cycle variants have been analyzed: reheating, partial cooling, partial cooling with reheating, intercooling, and intercooling with reheating. Partial derivatives of efficiency with respect to split ratio and intermediate pressure have been determined and set equal to zero to find optimum split ratio and intermediate pressure. This process has isolated the system's response to these two key parameters while keeping other cycle variables constant. Across all configurations, following parameters have been fixed: inlet temperatures of 550 °C and 32 °C for turbine and compressor components, an energy source temperature of 600 °C, an ambient temperature of 27 °C, and pressure limits of 75 bar and 200 bar. Optimization results show that recompression–reheating cycle achieves the highest efficiency of 39.62% at an optimum intermediate pressure of 139.43 bar and a split ratio of 71.1%. Recompression–partial cooling cycle exhibits the lowest maximum efficiency at 37.35%, with an optimum intermediate pressure of 85.87 bar and a split ratio of 62.6%. Recompression–partial cooling with reheating cycle reaches a maximum efficiency of 37.98% at an optimum intermediate pressure of 123.94 bar and a split ratio of 67.2%, while the intercooling cycle and intercooling with reheating cycle attain 39.57% at an optimum intermediate pressure of 80.03 bar and a split ratio of 66.4% and 39.59% at an optimum intermediate pressure of 116.1 bar and a split ratio of 69.2%, respectively. Additionally, exergy destruction has been calculated for all components of the system and it is related to thermal efficiency of the cycle.
[DOI: 10.1115/1.4066683]

Keywords: energy efficiency, exergy, optimization

1 Introduction

Supercritical power plants are operated near or above the working fluid's critical point, where small temperature or pressure changes result in abrupt changes to thermophysical properties. This sensitivity enables high efficiencies within compact designs consequently reducing both capital and operational costs in the energy industry [1–8]. Efficiency can be further enhanced by adjusting parameters such as intermediate pressure and split ratio. Sensitivity of these cycles to such parameters has been highlighted in previous studies [9–13]. Various recompression cycle configurations have been investigated in this research, including those with additional compression–cooling stages and turbine reheating. These configurations have been selected for their potential to enhance cycle performance under different operational conditions [14–19]. This study has aimed to maximize cycle efficiency by identifying optimum parameter values. Simulation and optimization processes have been integrated as follows: Newton–Rhapson iterative method has been employed to calculate temperatures throughout the cycle which forms the core of our simulation model. Two key optimization variables, intermediate pressure and split ratio, have been systematically adjusted to explore their impact on efficiency. To find the optimum values of these variables, partial derivatives of thermal efficiency with respect to split ratio and intermediate pressure have been derived and set equal to zero. Brent's algorithm [20] from the SciPy library [21] has been utilized to find the roots of the efficiency derivative with respect to each variable individually. This approach was adopted due to challenges encountered when attempting to directly apply Newton–Raphson method for a simultaneous optimization solution, which arose from extremely small second-order derivatives of efficiency. Thermophysical properties and derivative data have been obtained from NIST databases using the CoolProp library. Also, exergy analysis has been conducted to present exergy destruction at each component. Mathematical approach is detailed in Sec. 2 which introduces thermodynamic models and derivative equations for the analyses.

[1]Corresponding author.
Manuscript received August 4, 2024; final manuscript received August 26, 2024; published online October 11, 2024. Special. Editor: Hamid Hamidzedeh.

Section 3 presents results showing how intermediate pressure and split ratio affect the maximum efficiency of various cycle configurations. It also shows exergy analyses. Section 4 presents the concluding remarks.

2 Thermodynamics Model

Efficiency of a given thermodynamics cycle is given by

$$\eta_{th} = 1 - \frac{q_{out}}{q_{in}} \tag{1}$$

where q_{in} is energy input by heat interaction to intermediate energy exchangers and q_{out} is energy rejection by heat interaction from precoolers.

Derivatives of efficiency with respect to intermediate pressure and split ratio are given by

$$\frac{\partial \eta}{\partial r_s} = -\frac{1}{q_{in}^2}\left(\frac{\partial q_{out}}{\partial r_s} q_{in} - \frac{\partial q_{in}}{\partial r_s} q_{out}\right) \tag{2}$$

$$\frac{\partial \eta}{\partial P_{int}} = -\frac{1}{q_{in}^2}\left(\frac{\partial q_{out}}{\partial P_{int}} q_{in} - \frac{\partial q_{in}}{\partial P_{int}} q_{out}\right) \tag{3}$$

where r_s is the split ratio, proportion of the total mass flowrate that is directed to the main compressor after a cooling stage. It represents the fraction of the cooled fluid that continues through the main compression path. P_{int} is the intermediate pressure that determines the pressure ratio on the compressor–cooling and turbine–reheating sides.

Partial derivatives of energy interactions with respect to split ratio and intermediate pressure are given by

$$\frac{\partial q_{in}}{\partial r_s} = \frac{\partial}{\partial r_s}\left(\sum \Delta h_{in}\right) \tag{4}$$

$$\frac{\partial q_{out}}{\partial r_s} = \frac{\partial}{\partial r_s}\left(\sum \Delta h_{out}\right) \tag{5}$$

$$\frac{\partial q_{in}}{\partial P_{int}} = \frac{\partial}{\partial P_{int}}\left(\sum \Delta h_{in}\right) \tag{6}$$

$$\frac{\partial q_{out}}{\partial P_{int}} = \frac{\partial}{\partial P_{int}}\left(\sum \Delta h_{out}\right) \tag{7}$$

where Δh_{out} is the enthalpy differences across the precoolers and Δh_{in} is the enthalpy differences around the intermediate energy exchangers. Split ratio influences q_{out} terms related to the precooler depending on the cycle configuration. In layouts where the precooler cools the split flow, split ratio is directly involved in these calculations. Conversely, when a precooler is positioned before the flow split, split ratio does not factor into the Δh_{out} terms for the precooler.

First derivatives of enthalpy with respect to temperature and pressure are calculated:

$$h = h(T, P) \tag{8}$$

$$dh = \left(\frac{\partial h}{\partial T}\right)_P dT + \left(\frac{\partial h}{\partial P}\right)_T dP \tag{9}$$

Partial derivative of enthalpy with respect to split ratio for constant pressures is calculated:

$$\frac{\partial h}{\partial r_s} = \left(\frac{\partial h}{\partial T}\right)_P \left(\frac{dT}{dr_s}\right) \tag{10}$$

Partial derivative of enthalpy with respect to intermediate pressure is calculated:

$$\frac{\partial h}{\partial P_{int}} = \left(\frac{\partial h}{\partial T}\right)_{P_{int}} \left(\frac{dT}{dP_{int}}\right) + \frac{\partial h}{\partial P_{int}} \tag{11}$$

When the pressure of the state is constant, derivative of enthalpy with respect to intermediate pressure is calculated:

$$\frac{\partial h}{\partial P_{int}} = \left(\frac{\partial h}{\partial T}\right)_P \left(\frac{dT}{dP_{int}}\right) \tag{12}$$

The central finite difference formula for the change of temperature with respect to split ratio and intermediate pressure is given by

$$\frac{dT}{dr_s} = \frac{T(r_s + r_s) - T(r_s - r_s)}{2r_s} \tag{13}$$

$$\frac{dT}{dP_{int}} = \frac{T(P_{int} + P_{int}) - T(P_{int} - P_{int})}{2P_{int}} \tag{14}$$

An adaptive step size method is implemented in optimizing intermediate pressure. Efficiency derivatives with respect to intermediate pressure become extremely small, 10^{-11} to 10^{-15} depending on cycle configuration. Initially, a default step size of 0.1% of current intermediate pressure is used without prior information. Subsequent iterations assess changes in efficiency derivatives from previous steps. Step size adjusts inversely based on these changes such that large changes result in reduced step size, and small changes lead to increased step size.

Five different recompression cycles for supercritical carbon dioxide has been used, and they are: recompression–reheating, recompression–partial cooling, recompression–partial cooling with reheating, recompression–intercooling, and recompression–intercooling with reheating. Partial derivatives of thermal efficiencies with respect to split ratio and intermediate pressures are derived next.

For recompression–reheating cycle, Fig. 1, energy addition at the intermediate energy exchangers and energy rejection at the precooler are described by the following equations:

$$q_{in} = h_6(T_6, P_h) - h_5(T, P_h) + h_{16}(T_{16}, P_{int}) - h_{15}(T, P_{int}) \tag{15}$$

$$q_{out} = r_s(h_{10}(T, P_l) - h_1(T_1, P_l)) \tag{16}$$

Efficiency derivatives with respect to split ratio and intermediate pressure are then given by

$$\frac{\partial \eta}{\partial r_s} = -\frac{1}{q_{in}^2}\begin{pmatrix} \left((r_s)\left(\frac{\partial h_{10}}{\partial T_{10}}\right)|_{P_l} \frac{dT_{10}}{dr_s} + (h_{10} - h_1)\right) q_{in} - \\ \left(-\left(\frac{\partial h_5}{\partial T_5}\right)|_{P_h} \frac{dT_5}{dr_s} - \left(\frac{\partial h_{15}}{\partial T_{15}}\right)|_{P_{int}} \frac{dT_{15}}{dr_s}\right) q_{out} \end{pmatrix} \tag{17}$$

$$\frac{\partial \eta}{\partial P_{int}} = -\frac{1}{q_{in}^2}\begin{pmatrix} \left((r_s)\left(\frac{\partial h_{10}}{\partial T_{10}}\right)|_{P_l} \frac{dT_{10}}{dP_{int}}\right) q_{in} - \\ \left(-\left(\frac{\partial h_5}{\partial T_5}\right)|_{P_h} \frac{dT_5}{dP_{int}} + \frac{\partial h_{16}}{\partial P_{int}}|_{T_{16}} - \frac{\partial h_{15}}{\partial T_{15}}|_{P_{int}} \frac{dT_{15}}{dP_{int}} + \frac{\partial h_{15}}{\partial P_{int}}|_{T_{15}}\right) q_{out} \end{pmatrix} \tag{18}$$

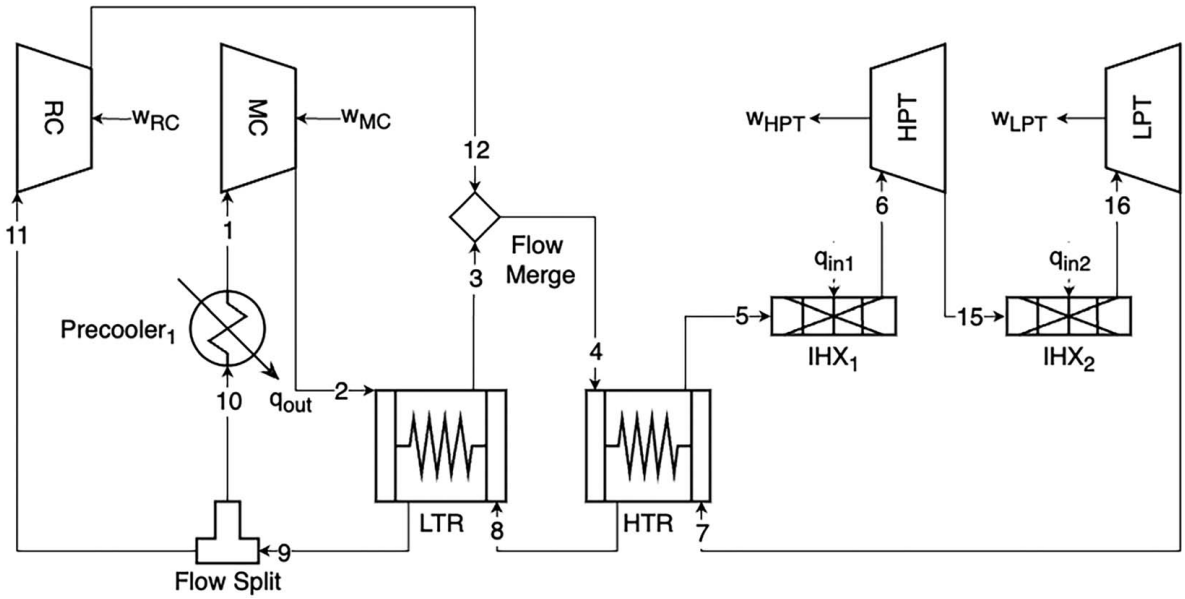

Fig. 1 Schematic diagram of reheating cycle (recompression–reheating cycle)

For recompression–partial cooling cycle, Fig. 2, energy addition at the energy exchanger and energy rejection at the precoolers are described by the following equations:

$$q_{in} = h_6(T_6, P_h) - h_5(T, P_l) \tag{19}$$

$$q_{out} = (r_s)(\, h_{10}(T, P_{int}) - h_1(T_1, P_{int})) + \; h_9(T, P_l) - h_{13}(T_{13}, P_l) \tag{20}$$

Efficiency derivatives with respect to split ratio and intermediate pressure is then given by

$$\frac{\partial \eta}{\partial r_s} = -\frac{1}{q_{in}^2}\left(\begin{array}{c}\left((r_s)\left(\frac{\partial h_{10}}{\partial T_{10}}\right)|_{P_{int}}\frac{dT_{10}}{dr_s} + (h_{10} - h_1) + \left(\frac{\partial h_9}{\partial T_9}\right)|_{P_{int}}\frac{dT_9}{dr_s}\right)q_{in} - \\ \left(-\left(\frac{\partial h_5}{\partial T_5}\right)|_{P_h}\frac{dT_5}{dr_s}\right)q_{out}\end{array}\right) \tag{21}$$

$$\frac{\partial \eta}{\partial P_{int}} = -\frac{1}{q_{in}^2}\left(\begin{array}{c}\left((r_s)\left(\frac{\partial h_{10}}{\partial T_{10}}|_{P_{int}}\frac{dT_{10}}{dP_{int}} + \frac{\partial h_{10}}{\partial P_{int}}|_{T_{10}} - \frac{\partial h_1}{\partial P_{int}}|_{T_1}\right) + \left(\frac{\partial h_9}{\partial T_9}|_{P_l}\frac{dT_9}{dP_{int}}\right)\right)q_{in} - \\ \left(-\left(\frac{\partial h_5}{\partial T_5}\right)|_{P_h}\frac{dT_5}{dP_{int}}\right)q_{out}\end{array}\right) \tag{22}$$

For partial cooling with reheating cycle, Fig. 3, energy addition at the energy exchangers and energy rejection at the precoolers are described by the following equations:

$$q_{in} = h_6(T_6, P_h) - h_5(T, P_h) + \; h_{16}(T_{16}, P_{int}) - h_{15}(T, P_{int}) \tag{23}$$

$$q_{out} = r_s(\, h_{10}(T, P_{int}) - h_1(T_1, P_{int})) + \; h_9(T, P_l) - h_{13}(T_{13}, P_l) \tag{24}$$

Efficiency derivatives with respect to split ratio and intermediate pressure are then given by

$$\frac{\partial \eta}{\partial r_s} = -\frac{1}{q_{in}^2}\left(\begin{array}{c}\left((r_S)\left(\frac{\partial h_{10}}{\partial T_{10}}|_{P_{int}}\frac{dT_{10}}{dr_s}\right) + (\, h_{10} - h_1) + \left(\frac{\partial h_9}{\partial T_9}\right)|_{P_{int}}\frac{dT_9}{dr_s}\right)q_{in} - \\ \left(-\left(\frac{\partial h_5}{\partial T_5}\right)|_{P_h}\frac{dT_5}{dr_s} - \left(\frac{\partial h_{15}}{\partial T_{15}}\right)|_{P_{int}}\frac{dT_{15}}{dr_s}\right)q_{out}\end{array}\right) \tag{25}$$

$$\frac{\partial \eta}{\partial P_{int}} = -\frac{1}{q_{in}^2}\left(\begin{array}{c}\left((r_s)\left(\frac{\partial h_{10}}{\partial T_{10}}|_{P_{int}}\frac{dT_{10}}{dP_{int}} + \frac{\partial h_{10}}{\partial P_{int}}|_{T_{10}} - \frac{\partial h_1}{\partial P_{int}}|_{T_1}\right) + \left(\frac{\partial h_9}{\partial T_9}|_{P_l}\frac{dT_9}{dP_{int}}\right)\right)q_{in} - \\ \left(-\left(\frac{\partial h_5}{\partial T_5}\right)|_{P_h}\frac{dT_5}{dP_{int}} + \frac{\partial h_{16}}{\partial P_{int}}|_{T_{16}} - \frac{\partial h_{15}}{\partial T_{15}}|_{P_{int}}\frac{dT_{15}}{dP_{int}} + \frac{\partial h_{15}}{\partial P_{int}}|_{T_{15}}\right)q_{out}\end{array}\right) \tag{26}$$

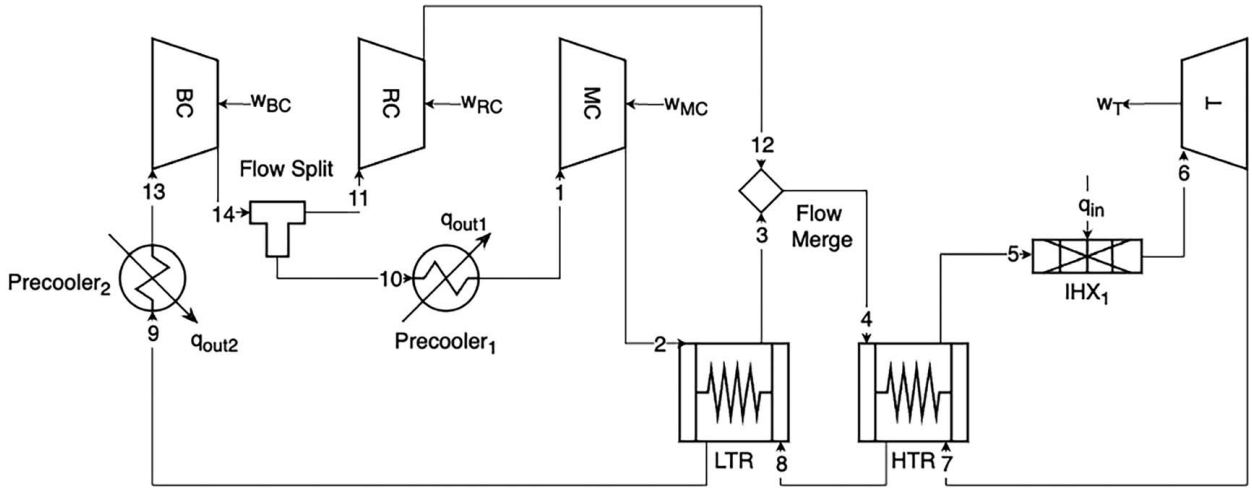

Fig. 2 Schematic diagram of partial cooling cycle (recompression–partial cooling cycle)

For recompression–intercooling cycle, Fig. 4, energy addition at the energy exchanger and energy rejection at the precoolers are described by the following equations:

$$q_{in} = h_6(T_6, P_h) - h_5(T, P_l) \tag{27}$$

$$q_{out} = (r_s)((\ h_{10}(T, P_l) - h_{13}(T_1, P_l)) + \ h_{14}(T, P_{int}) - h_1(T_1, P_{int})) \tag{28}$$

Efficiency derivatives with respect to split ratio and intermediate pressure is then given by

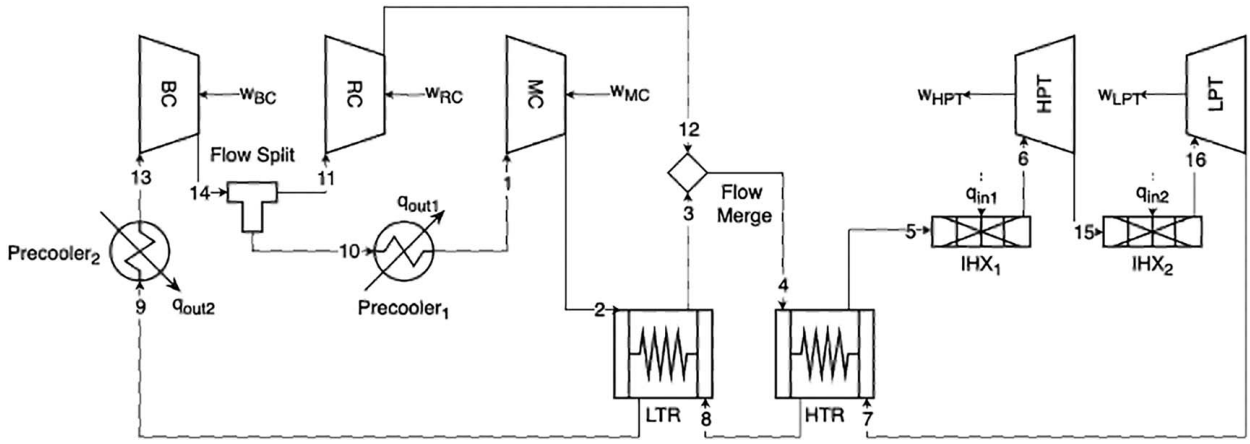

Fig. 3 Schematic diagram of partial cooling with reheating cycle (recompression–partial cooling with reheating cycle)

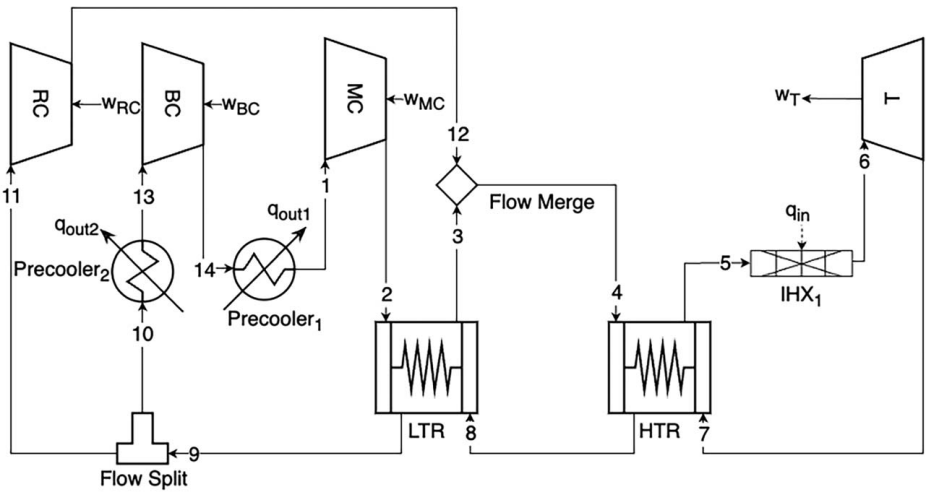

Fig. 4 Schematic diagram of intercooling cycle (recompression–intercooling cycle)

$$\frac{\partial \eta}{\partial r_s} = -\frac{1}{q_{\text{in}}^2}\left(\begin{array}{c}\left((r_s)\left(\left(\frac{\partial h_{10}}{\partial T_{10}}\right)|_{P_l}\frac{dT_{10}}{dr_s} + \left(\frac{\partial h_{14}}{\partial T_{14}}\right)|_{P_{\text{int}}}\frac{dT_{14}}{dr_s}\right) + (h_{10} - h_{13} + h_{14} - h_1)\right)q_{\text{in}} - \\ \left(-\left(\frac{\partial h_5}{\partial T_5}\right)|_{P_h}\frac{dT_5}{dr_s}\right)q_{\text{out}}\end{array}\right) \tag{29}$$

$$\frac{\partial \eta}{\partial P_{\text{int}}} = -\frac{1}{q_{\text{in}}^2}\left(\begin{array}{c}(r_s)\left(\frac{\partial h_{10}}{\partial T_{10}}|_{P_l}\frac{dT_{10}}{dP_{\text{int}}} + \frac{\partial h_{14}}{\partial T_{14}}|_{P_{\text{int}}}\frac{dT_{14}}{dP_{\text{int}}} + \frac{\partial h_{14}}{\partial P_{\text{int}}}|_{T_{14}} - \frac{\partial h_1}{\partial P_{\text{int}}}|_{T_1}\right)q_{\text{in}} - \\ \left(-\left(\frac{\partial h_5}{\partial T_5}\right)|_{P_h}\frac{dT_5}{dP_{\text{int}}}\right)q_{\text{out}}\end{array}\right) \tag{30}$$

For recompression–intercooling with reheating cycle, Fig. 5, energy addition at the energy exchangers and energy rejection at the precoolers are described by the following equations:

$$q_{\text{in}} = h_6(T_6, P_h) - h_5(T, P_h) + h_{16}(T_{16}, P_{\text{int}}) - h_{15}(T, P_{\text{int}}) \tag{31}$$

$$q_{\text{out}} = (r_s)((h_{10}(T, P_l) - h_{13}(T_1, P_l)) + h_{14}(T, P_{\text{int}}) - h_1(T_1, P_{\text{int}})) \tag{32}$$

Efficiency derivatives with respect to split ratio and intermediate pressure is given by

$$\frac{\partial \eta}{\partial r_s} = -\frac{1}{q_{\text{in}}^2}\left(\begin{array}{c}\left(\left(\frac{\partial h_{10}}{\partial T_{10}}\right)|_{P_l}\frac{dT_{10}}{dr_s} + \left(\frac{\partial h_{14}}{\partial T_{14}}\right)|_{P_{\text{int}}}\frac{dT_{14}}{dr_s}\right) + (h_{10} - h_{13} + h_{14} - h_1)q_{\text{in}} - \\ \left(-\left(\frac{\partial h_5}{\partial T_5}\right)|_{P_h}\frac{dT_5}{dr_s} - \left(\frac{\partial h_{15}}{\partial T_{15}}\right)|_{P_{\text{int}}}\frac{dT_{15}}{dr_s}\right)q_{\text{out}}\end{array}\right) \tag{33}$$

$$\frac{\partial \eta}{\partial P_{\text{int}}} = -\frac{1}{q_{\text{in}}^2}\left(\begin{array}{c}(r_s)\left(\frac{\partial h_{10}}{\partial T_{10}}|_{P_l}\frac{dT_{10}}{dP_{\text{int}}} + \frac{\partial h_{14}}{\partial T_{14}}|_{P_{\text{int}}}\frac{dT_{14}}{dP_{\text{int}}} + \frac{\partial h_{14}}{\partial P_{\text{int}}}|_{T_{14}} - \frac{\partial h_1}{\partial P_{\text{int}}}|_{T_1}\right)q_{\text{in}} - \\ \left(-\left(\frac{\partial h_5}{\partial T_5}\right)|_{P_h}\frac{dT_5}{dP_{\text{int}}} + \frac{\partial h_{16}}{\partial P_{\text{int}}}|_{T_{16}} - \frac{\partial h_{15}}{\partial T_{15}}|_{P_{\text{int}}}\frac{dT_{15}}{dP_{\text{int}}} + \frac{\partial h_{15}}{\partial P_{\text{int}}}|_{T_{15}}\right)q_{\text{out}}\end{array}\right) \tag{34}$$

3 Results

Results present analyses of five different supercritical carbon dioxide cycle configurations. For each configuration, key results are provided: maximum efficiency and optimum intermediate pressure across different split ratios, maximum efficiency and optimum split ratio across different intermediate pressures. All configurations show transitional states related to the properties of the supercritical carbon dioxide and the influence of split ratio in recuperators. The analysis is conducted under a set of constant parameters that are shown in Table 1.

3.1 Recompression–Reheating Cycle. Figure 6 shows results for maximum efficiency and corresponding optimum intermediate pressure as a function of split ratio for recompression–reheating cycle. Blue curve represents maximum efficiency at each split ratio. It demonstrates a clear peak at 71.1%. As it can be seen efficiency increases steadily with split ratio until reaching its maximum value of 39.62%. After this peak, it gradually declines. The dotted curve indicates the optimum intermediate pressure corresponding to the maximum efficiency at any split ratio. Optimum intermediate pressure changes slightly for split ratio of less than 71%. It drops drastically at split ratio of 72%. It continues to decrease slightly

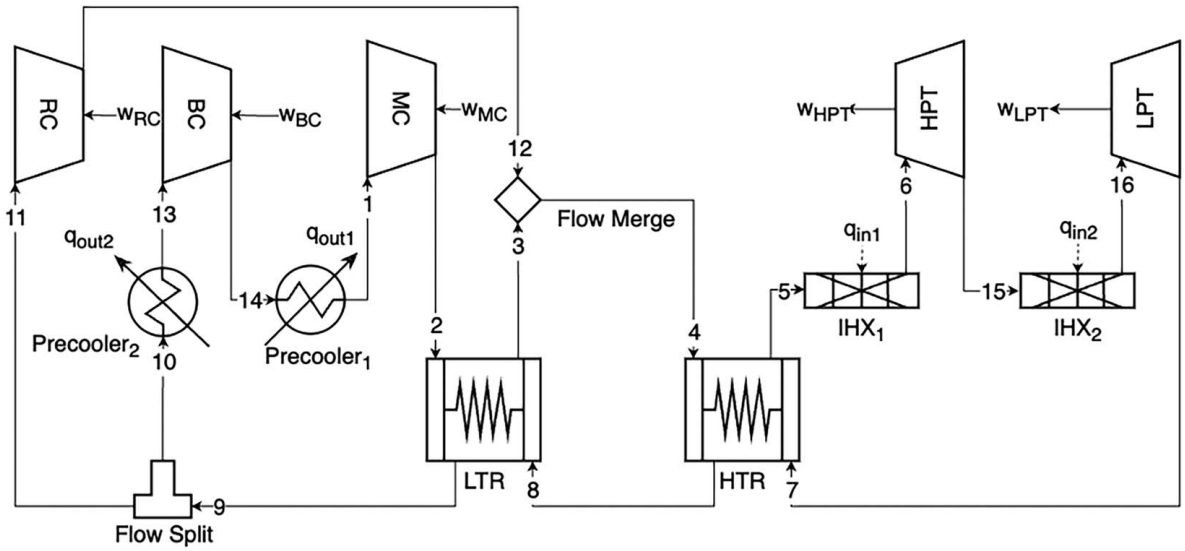

Fig. 5 Schematic diagram of intercooling with reheating cycle (recompression–intercooling with reheating cycle)

Table 1 Constant parameters and their values

Parameter	Value
Compressors isentropic efficiency (η_{comp})	0.85
Turbine isentropic efficiency (η_{turb})	0.85
Effectiveness of low temperature recuperator (ϵ_{LTR})	0.85
Effectiveness of high temperature recuperator (ϵ_{HTR})	0.85
Precooler outlet temperature (T_{min})	32 °C
Turbine inlet temperature (T_{max})	550 °C
Low pressure (P_{low})	75 bar
High pressure (P_{high})	200 bar
Ambient temperature (T_o)	27 °C
Source temperature (T_s)	600 °C
Intermediate pressure (P_{int})	[P_{low}, P_{high}] increment = 10^2 Pa
Split ratio (r_s)	0.3–1.0 increment = 10^{-4}

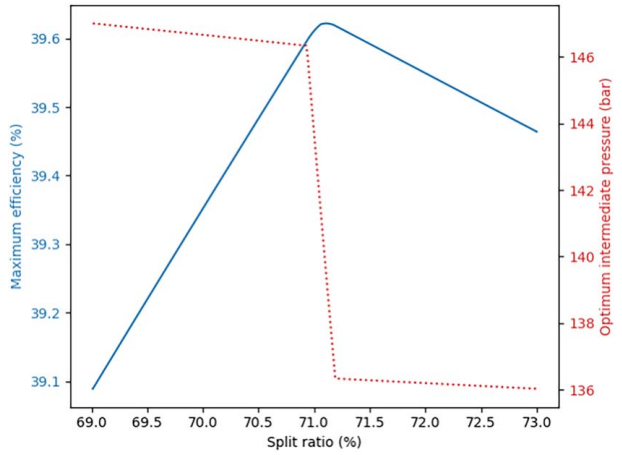

Fig. 6 Maximum efficiency and optimum intermediate pressure across different split ratios in reheating cycle

as the split ratio increases further. The peak of maximum efficiency corresponds to an optimum intermediate pressure of 139.39 bar.

Figure 7 shows results for maximum efficiency and optimum split ratio across different intermediate pressures for recompression–reheating cycle. Maximum efficiency initially rises with increasing intermediate pressure then gradually declines. Optimum split ratio shows an inverse relationship with intermediate pressure decreasing from 71.3% at 130 bar to 70.4% at 180 bar. The highest efficiency is achieved at a split ratio of 71.1%, corresponding to the peak of maximum efficiency curve.

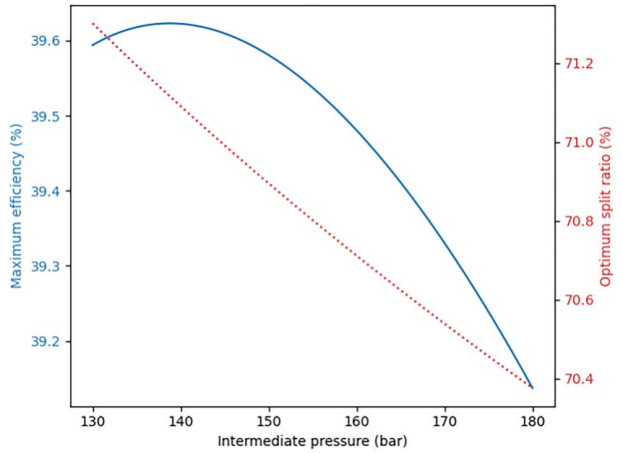

Fig. 7 Maximum efficiency and optimum split ratio across different intermediate pressures in reheating cycle

3.2 Recompression–Partial Cooling Cycle. Figure 8 shows results for maximum efficiency and optimum intermediate pressures across different split ratios for recompression–partial cooling cycle. Maximum efficiency increases with split ratio reaching a peak of 37.35% at 62.6% split ratio. After this maximum, efficiency gradually declines as split ratio increases further. Optimum intermediate pressure remains constant at 80 bar for split ratios up to 62%. At the peak of maximum efficiency, optimum intermediate pressure jumps to 85.87 bar. Beyond this point, it continues to increase steadily as the split ratio grows.

Figure 9 shows results for maximum efficiency and optimum split ratio across different intermediate pressures for recompression–partial cooling cycle. Maximum efficiency initially rises with increasing intermediate pressure till its maximum value. Beyond this point, efficiency gradually declines as intermediate pressure increases further. Optimum split ratio increases from about 61.5% at 80 bar to 69.5% at 150 bar. The highest efficiency is achieved at a split ratio of 62.6% corresponding to the peak of the maximum efficiency curve.

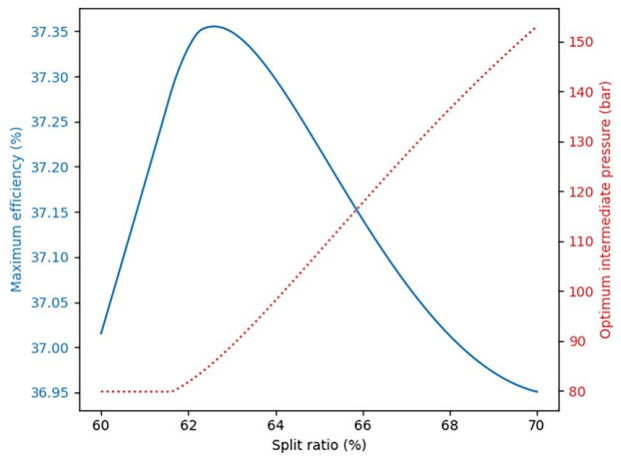

Fig. 8 Maximum efficiency and optimum intermediate pressure across different split ratios in partial cooling cycle

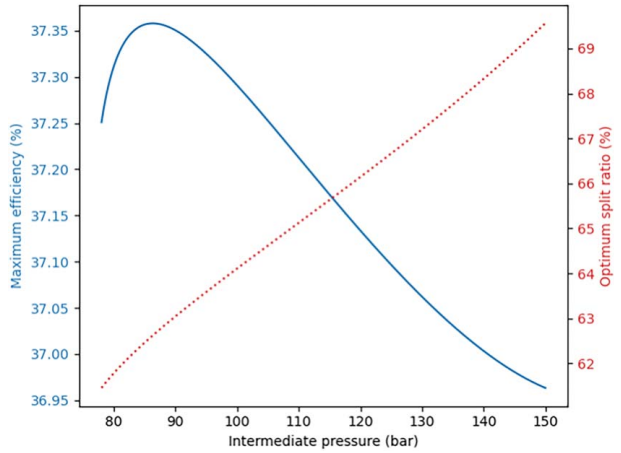

Fig. 9 Maximum efficiency and optimum split ratio across different intermediate pressures in partial cooling cycle

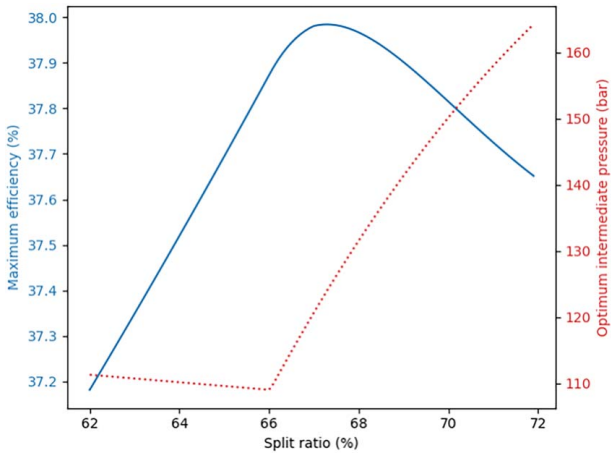

Fig. 10 Maximum efficiency and optimum intermediate pressure across different split ratios in partial cooling with reheating cycle

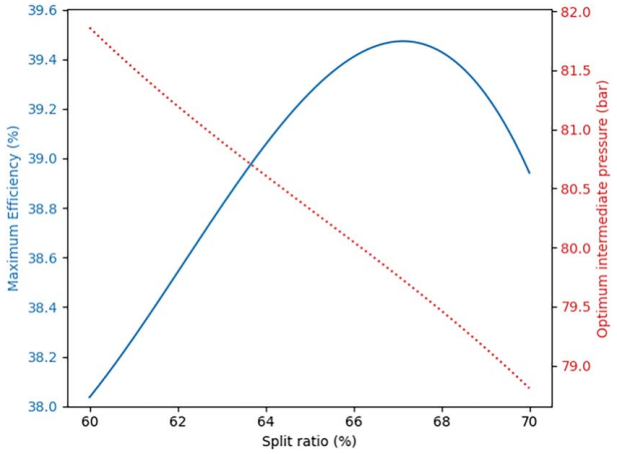

Fig. 12 Maximum efficiency and optimum intermediate pressure across different split ratios in intercooling cycle

3.3 Recompression–Partial Cooling With Reheating Cycle. Figure 10 shows results for maximum efficiency and optimum intermediate pressure across different split ratios for partial cooling with reheating cycle. Maximum efficiency increases with split ratio to a peak of 37.98% at 67% split ratio, before gradually declining. Optimum intermediate pressure remains relatively constant at about 110 bar for split ratios up to about 66%. At the point of maximum efficiency, optimum intermediate pressure is 123.94 bar. Beyond this point, it continues to increase steadily as the split ratio grows.

Figure 11 shows results for maximum efficiency and optimum split ratio across intermediate pressures for a recompression–partial cooling with reheating cycle. Maximum efficiency initially rises with increasing intermediate pressure. Beyond the peak point, efficiency gradually declines as intermediate pressure increases further. Optimum split ratio increases from about 64% at 80 bar to 70% at 150 bar. The highest efficiency is achieved at a split ratio of 67.2% corresponding to the peak of the maximum efficiency curve.

3.4 Recompression–Intercooling Cycle. Figure 12 shows results for maximum efficiency and corresponding optimum intermediate pressure across split ratios for recompression–intercooling cycle. Maximum efficiency increases with split ratio to a peak of 39.49% at 67.12% split ratio before gradually declining. Optimum intermediate pressure decreases steadily from about 82 bar at a 60% split ratio to approximately 79 bar at a 70% split ratio. At the peak of maximum efficiency, optimum intermediate pressure is 79.12 bar.

Figure 13 shows results for maximum efficiency and optimum split ratio across intermediate pressures for a recompression–intercooling cycle. Maximum efficiency initially rises with increasing intermediate pressure. Beyond the maximum efficiency, efficiency gradually declines as pressure increases further. Optimum split ratio increases from about 66.5% at 80 bar to 70.5% at 150 bar. The highest efficiency is achieved at a split ratio of 66.39% corresponding to the peak of the maximum efficiency of 39.47%.

3.5 Recompression–Intercooling With Reheating Cycle. Figure 14 shows results for maximum efficiency and optimum intermediate pressure across split ratios for a recompression–intercooling with reheating cycle. Maximum efficiency increases with split ratio, reaching a peak of 39.59% at 69.2% split ratio. After this maximum, efficiency gradually declines as split ratio increases further. Optimum intermediate pressure remains relatively stable around 110–113 bar for split ratios up to 69%. At the peak of maximum efficiency, optimum intermediate pressure increases to 116.34 bar.

Figure 15 shows results for maximum efficiency and optimum split ratios across intermediate pressures for a recompression–

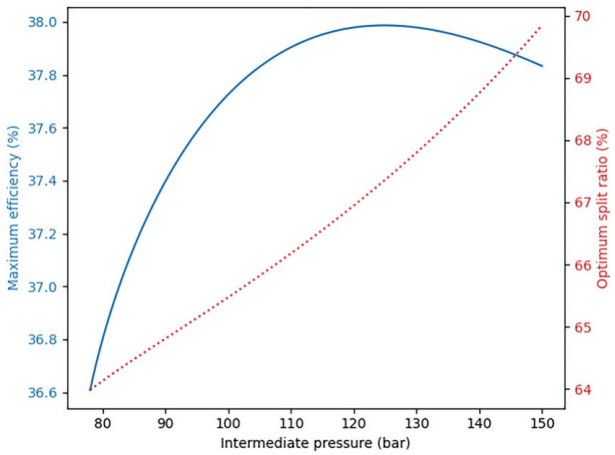

Fig. 11 Maximum efficiency and optimum split ratio across different intermediate pressures in partial cooling with reheating cycle

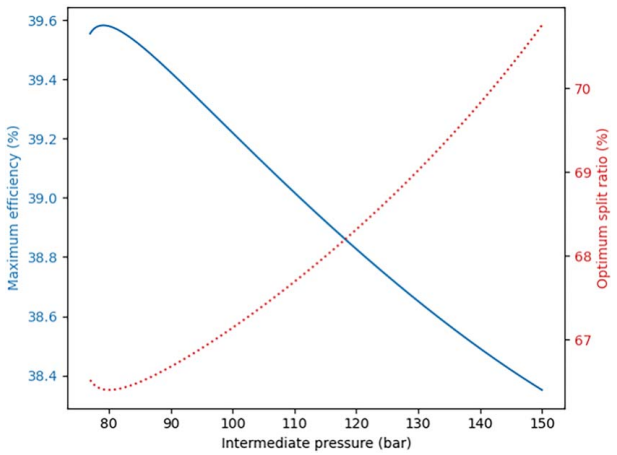

Fig. 13 Maximum efficiency and optimum split ratio across different intermediate pressures in intercooling cycle

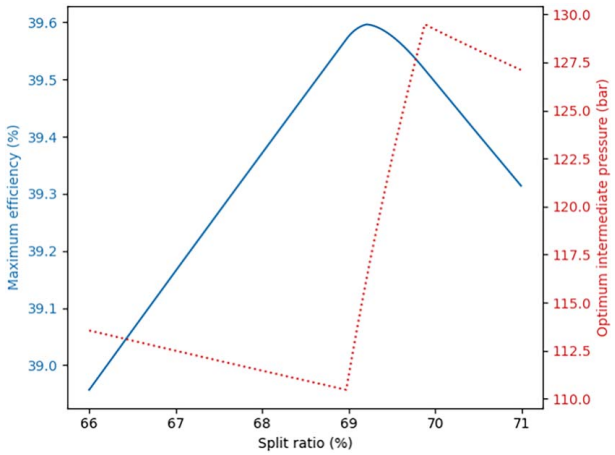

Fig. 14 Maximum efficiency and optimum intermediate pressure across different split ratios in Intercooling with reheating cycle

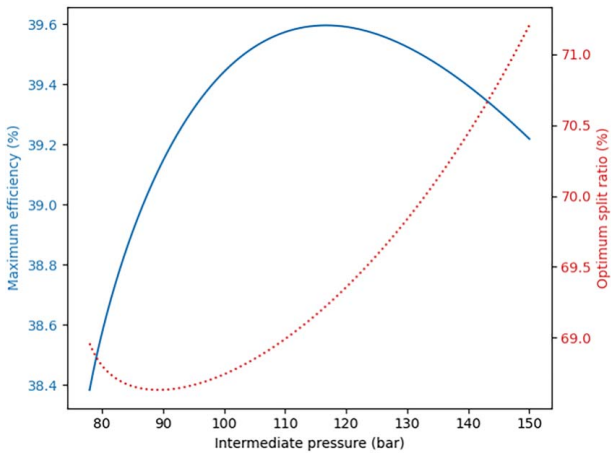

Fig. 15 Optimum split ratio across different intermediate pressures at a point of maximum efficiency in Intercooling with reheating cycle

intercooling with reheating cycle. Maximum efficiency rises with increasing intermediate pressure until reaching a peak and then gradually declines as pressure increases further. Optimum split ratio initially decreases slightly from its value at 80 bar, reaches a minimum, and then increases continuously as intermediate pressure rises to 150 bar. The highest efficiency is achieved at a split ratio of 69.20% corresponding to the peak of the maximum efficiency curve.

Table 2 presents the optimization results for optimum intermediate pressures and split ratios across variants of supercritical recompression cycle configurations. These results demonstrate the combination of intermediate pressure and split ratio that maximizes thermal efficiency for each cycle configuration.

Table 2 Optimization results for intermediate pressure and split ratio

Cycles	Optimum intermediate pressure (bar)	Optimum split ratio (%)	Maximum efficiency (%)
Recompression–reheating	139.43	71.1	39.62
Recompression–partial cooling	85.87	62.6	37.35
Recompression–partial cooling with reheating	123.94	67.3	37.98
Recompression–intercooling	79.42	67.1	39.47
Recompression–intercooling with reheating	116.1	69.2	39.59

3.6 Exergy Analysis. Exergy analysis provides insights into the thermodynamic inefficiencies of cycle components. This section presents the methodology and results of exergy analysis for the cycles.

General exergy balance equation is given by

$$\frac{d\Phi}{dt} = \dot{\Phi}_H - \dot{W}_{\text{net}}^{\text{useful}} + \sum_i \dot{m}_i \psi_i - \sum_e \dot{m}_e \psi_e - \dot{\Phi}_d \tag{35}$$

where Φ is exergy, $\dot{\Phi}_H$ is rate of exergy input by heat interaction from a source, ψ is flow exergy per unit mass, and $\dot{\Phi}_d$ is rate of exergy destruction. Rate of exergy input with constant source and ambient temperatures is given by

$$\dot{\Phi}_H = \int \delta\dot{Q}\left(1 - \frac{T_o}{T_S}\right) = \dot{Q}_{\text{in}}\left(1 - \frac{T_o}{T_s}\right) \tag{36}$$

General entropy balance equation is given by

$$\frac{dS}{dt} = \int \left(\frac{\delta\dot{Q}}{T}\right)_{\text{boundary}} + \sum_i \dot{m}_i s_i - \sum_e \dot{m}_e s_e - \dot{S}_{\text{gen}} \tag{37}$$

where S is entropy and s is entropy of a state per unit mass and $\dot{S}_{\text{gen}}$ is the rate of entropy generation. Finally, exergy destruction of each component has been calculated by

$$\dot{\Phi}_d = T_o \dot{S}_{\text{gen}} \tag{38}$$

To determine the relative impact of each component's inefficiency, exergy destruction percentages have been calculated. These percentages have been defined as the ratio of a component's exergy destruction to total exergy input of the cycle which correlates to exergetic efficiency of the cycle. Exergetic efficiency is given by the ratio of exergy output of the cycle to exergy input to the cycle:

$$\eta_{\text{ex}} = \frac{\dot{\Phi}_H - \dot{\Phi}_d}{\dot{\Phi}_H} = 1 - \frac{\dot{\Phi}_d}{\dot{\Phi}_H} \tag{39}$$

Table 3 presents the exergy destruction percentages for various components across all cycle configurations, calculated at the maximum efficiency point determined by the optimized intermediate pressure and split ratio values obtained in this study.

Order of exergy input from highest to lowest is: partial cooling with reheating (174.5 kJ/kg), partial cooling (169.7 kJ/kg), intercooling with reheating (152.9 kJ/kg), intercooling (140.8 kJ/kg), and reheating (136.7 kJ/kg) cycles. Exergy analyses show the combined recuperators consistently account for the highest proportion of exergy destruction in all cycles.

Partial cooling with reheating cycle, having the highest exergy input, shows significant losses in recuperators at 21.4% combined and intermediate energy exchanger IHX1 at 6.8%. Following that, partial cooling cycle demonstrates high exergy destruction in recuperators at 19.0% combined, IHX1 at 11.8%, and HPT at 5.4%.

Intercooling with reheating and intercooling cycles show moderate exergy input levels. The former has higher destruction in HTR at 11.9% and LTR at 7.8%, while the latter shows notable losses in IHX1 at 10.0%, HTR at 8.9%, and LTR at 7.1%.

Reheating cycle, with the lowest exergy input, exhibits better exergy utilization in some components but still has notable destruction in HTR at 7.2%, LTR at 7.4%, and IHX1 at 6.3%. Importantly, the highest exergy destruction after combined recuperators for the reheating cycle is in the precooler PRE1, accounting for 7.8% of exergy destruction.

Across all cycles, compressors MC, RC, BC, and mixing chamber MIX contribute to exergy destruction to varying degrees, but generally less than the other components in the cycle. Moreover,

Table 3 Percentage of exergy destructions with respect to the total exergy input to the cycle across different components

Cycles	PRE1	PRE2	IHX1	IHX2	LPT	HPT	LTR	HTR	MC	RC	BC	MIX	Total
Partial cooling and reheating (174.5 kJ/kg)	2.1	2.2	6.8	1.4	2.4	2.6	3.8	17.6	0.6	0.4	0.9	1.2	42.0
Partial cooling (169.7 kJ/kg)	0.9	3.0	11.8	–	–	5.4	2.8	16.2	0.9	0.7	0.4	1.0	43.1
Intercooling and reheating (152.9 kJ/kg)	2.1	2.3	5.0	2.0	2.2	3.5	7.8	11.9	0.8	1.3	0.6	0.2	39.7
Intercooling (140.8 kJ/kg)	0.6	3.8	10.0	–	–	6.5	7.1	8.9	1.3	1.6	0.07	0.02	39.89
Reheating (136.7 kJ/kg)	7.8	–	6.3	1.0	2.1	4.3	7.4	7.2	1.9	1.6	–	0.03	39.63

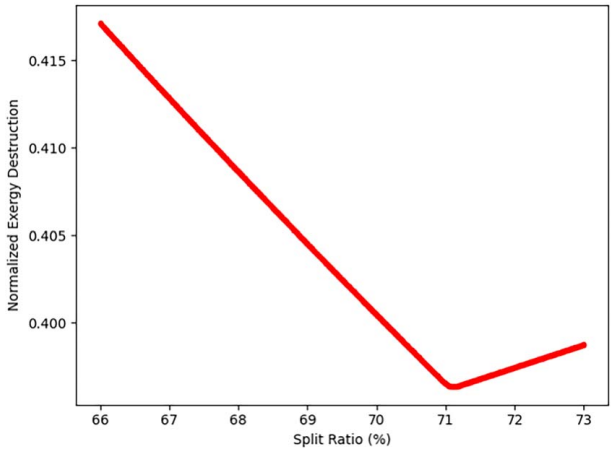

Fig. 16 Normalized exergy destruction as a function of split ratio at maximum efficiency

exergetic efficiency of each cycle has been calculated by subtracting the total exergy destruction percentages from 100%. Values ranging from 60.37% for reheating cycle to 56.9% for partialcooling cycle have been obtained. Intercooling with reheating, intercooling, and partial cooling with reheating cycles showed efficiencies of 60.3%, 60.11%, and 58.0%, respectively.

Figure 16 shows normalized exergy destruction as a function of split ratio at maximum efficiency for recompression–reheating cycle. Normalized exergy destruction has been calculated as the ratio of total exergy destruction across all components to the total exergy input to the cycle. It decreases with increasing split ratio until reaching a minimum value. This minimum point corresponds to the optimum split ratio identified in the cycle optimization study. The cycle efficiency is maximum at minimum exergy destruction. For the other four cycles, the same results have been determined.

4 Conclusion

This study has shown optimization of split ratio and intermediate pressure to maximize efficiency in various supercritical carbon dioxide recompression cycles. Additionally, exergy analysis has been performed across all cycles. The followings are the conclusions:

(1) Each cycle configuration exhibited a unique optimum combination of split ratio and intermediate pressure for maximum efficiency.
(2) Among the analyzed configurations, the reheating cycle achieved the highest efficiency of 39.62%, followed closely by the intercooling with reheating cycle at 39.59%. The intercooling cycle reached 39.47%, while the partial cooling with reheating and partial cooling cycles attained lower efficiencies of 37.98% and 37.35%, respectively.
(3) Step size in optimum intermediate pressure calculations becomes critical, particularly near the transitional points. As the system approaches these points, the precision required to accurately capture changes in temperatures across states in the cycle.
(4) Recuperators (LTR and HTR combined) accounted for the highest proportion of exergy destruction for the exergy input across all configurations, ranging from 14.6% in the reheating cycle to 21.4% in the partial cooling and reheating cycle. The partial cooling cycle showed 19.0%, intercooling with reheating cycle 19.7%, and intercooling cycle 16.0% exergy destruction in recuperators.
(5) Analysis of the reheating cycle revealed that the normalized sum of exergy destruction across all components, calculated at the point of maximum efficiency for each split ratio, reaches its minimum at the cycle's optimum split ratio of 71.1%. This finding shows direct correlation between maximum efficiency and minimum exergy destruction in the cycle. The same situation happens in all cycles.

Conflict of Interest

There are no conflicts of interest. This article does not include research in which human participants were involved. Informed consent is not applicable. This article does not include any research in which animal participants were involved.

Data Availability Statement

The datasets generated and supporting the findings of this article are obtainable from the corresponding author upon reasonable request.

References

[1] Dostal, V., Hejzlar, P., and Driscoll, M. J., 2006, "The Supercritical Carbon Dioxide Power Cycle: Comparison to Other Advanced Power Cycles," Nucl. Technol., **154**(3), pp. 283–301.
[2] Ahn, Y., Bae, S. J., Kim, M., Cho, S. K., Baik, S., Lee, J. I., and Cha, J. E., 2015, "Review of Supercritical CO_2 Power Cycle Technology and Current Status of Research and Development," Nucl. Eng. Technol., **47**(6), pp. 647–661.
[3] Turchi, C. S., Ma, Z., Neises, T. W., and Wagner, M. J., 2013, "Thermodynamic Study of Advanced Supercritical Carbon Dioxide Power Cycles for Concentrating Solar Power Systems," ASME J. Sol. Energy Eng., **135**(4), p. 041007.
[4] Musgrove, G., and Wright, S., 2017, "1—Introduction and Background," *Fundamentals and Applications of Supercritical Carbon Dioxide (sCO_2) Based Power Cycles*, K. Brun, P. Friedman, and R. Dennis, eds., Woodhead Publishing, Duxford, UK, pp. 1–22.
[5] Wright, S. A., Radel, R. F., Vernon, M. E., Pickard, P. S., and Rochau, G. E., 2010, *Operation and Analysis of a Supercritical CO2 Brayton Cycle*, Sandia National Laboratories (SNL), Albuquerque, NM, and Livermore, CA (United States), p. SAND2010-0171.
[6] Crespi, F., Rodríguez de Arriba, P., Sánchez, D., Ayub, A., Di Marcoberardino, G., Invernizzi, C. M., Martínez, G. S., et al., 2022, "Thermal Efficiency Gains Enabled by Using CO2 Mixtures in Supercritical Power Cycles," Energy, **238**, p. 121899.
[7] Tatli, A. E., You, D., Ghanavati, A., and Metghalchi, H., 2023, "Insight Into Recompression Brayton Cycle," ASME Open J. Eng., **2**, p. 021023.
[8] You, D., and Metghalchi, H., 2021, "On the Supercritical Carbon Dioxide Recompression Cycle," ASME J. Energy Resour. Technol., **143**(12), p. 121701.
[9] Tatli, A. E., You, D., and Metghalchi, H., 2024, "Effects of Intermediate Pressure and Split Ratio on Supercritical Modified Recompression Cycles Performance," ASME Open J. Eng., **3**, p. 031015.
[10] Nassar, A., Moroz, L., Burlaka, M., Pagur, P., and Govoruschenko, Y., 2015, "Designing Supercritical CO2 Power Plants Using an Integrated Design System," presented at the ASME 2014 Gas Turbine India Conference, American Society of Mechanical Engineers Digital Collection.

[11] Moisseytsev, A., and Sienicki, J. J., 2007, *Development of a Plant Dynamics Computer Code for Analysis of a Supercritical Carbon Dioxide Brayton Cycle Energy Converter Coupled to a Natural Circulation Lead-Cooled Fast Reactor*, Argonne National Lab. (ANL), Argonne, IL (United States), p. ANL-06/27.
[12] Moore, J., Brun, K., Evans, N., and Kalra, C., 2015, "Development of 1 MWe Supercritical CO2 Test Loop," Proceedings of the ASME Turbo Expo 2015: Turbine Technical Conference and Exposition, in Oil and Gas Applications; Supercritical CO_2 Power Cycles; Wind Energy, vol. 9, Montreal, Quebec, Canada, June 15–19, ASME, pp. 1–11.
[13] Novales, D., Erkoreka, A., De la Peña, V., and Herrazti, B., 2019, "Sensitivity Analysis of Supercritical CO_2 Power Cycle Energy and Exergy Efficiencies Regarding Cycle Component Efficiencies for Concentrating Solar Power," Energy Convers. Manage., **182**, pp. 430–450.
[14] You, D., and Metghalchi, H., 2022, "Analysis of Aqueous Lithium Bromide Absorption Refrigeration Systems," ASME J. Energy Resour. Technol., **144**(1), p. 012105.
[15] You, D., Tatli, A. E., Ghanavati, A., and Metghalchi, H., Nov. 2022, "Design and Analysis of a Solar Energy Driven Tri-Generation Plant for Power, Heating, and Refrigeration," ASME J. Energy Resour. Technol., **144**(8), p. 082105.
[16] Vasquez Padilla, R., Soo Too, Y. C., Benito, R., McNaughton, R., and Stein, W., 2018, "Multi-Objective Thermodynamic Optimisation of Supercritical CO_2 Brayton Cycles Integrated With Solar Central Receivers," Int. J. Sustain. Energy, **37**(1), pp. 1–20.
[17] Ruiz-Casanova, E., Rubio-Maya, C., Pacheco-Ibarra, J. J., Ambriz-Díaz, V. M., Romero, C. E., and Wang, X., 2020, "Thermodynamic Analysis and Optimization of Supercritical Carbon Dioxide Brayton Cycles for Use With Low-Grade Geothermal Heat Sources," Energy Convers. Manage., **216**, p. 112978.
[18] Wang, K., He, Y.-L., and Zhu, H.-H., 2017, "Integration Between Supercritical CO_2 Brayton Cycles and Molten Salt Solar Power Towers: A Review and a Comprehensive Comparison of Different Cycle Layouts," Appl. Energy, **195**, pp. 819–836.
[19] Kim, Y. M., Kim, C. G., and Favrat, D., 2012, "Transcritical or Supercritical CO_2 Cycles Using Both Low- and High-Temperature Heat Sources," Energy, **43**(1), pp. 402–415.
[20] Brent, R. P., 1971, "An Algorithm With Guaranteed Convergence for Finding a Zero of a Function," Comput. J., **14**(4), pp. 422–425.
[21] Virtanen, P., Oliphant, T. E., Haberland, M., Reddy, T., Cournapeau, D., Brovski, E., Peterson, P., et al., 2020, "SciPy 1.0: Fundamental Algorithms for Scientific Computing in Python," Nat. Methods, **17**(3), p. Art. no. LA-UR-19-29085.